Effects of Kinetics Coefficients on Ternary Phase Separation During the Wet Spinning Process

Yu Han, Jun Wang, Hongdong Zhang

Department of Macromolecular Science, Fudan University, Shanghai 200433, China

Received 4 September 2011; accepted 10 November 2011
DOI 10.1002/app.36478
Published online in Wiley Online Library (wileyonlinelibrary.com).

ABSTRACT: A new Monte Carlo diffusion model is employed to simulate the phase separation of the ternary system during wet spinning process. Our results illustrate the thermodynamics parameters are the primary factors in morphology determination during the phase separation process. Meanwhile by varying kinetic parameters different fiber structures ranging from dust-like, finger-like to sponge-like morphologies are obtained. The morphological patterns are discussed in relation to the rate of particle exchange and the phase diagram. On the basis of the systematical simulation experiments we propose how the competition between segment–solvent and solvent–nonsolvent exchange determines the ultimate fiber morphologies in spinning solution.© 2012 Wiley Periodicals, Inc. J Appl Polym Sci 000: 000–000, 2012

Key words: kinetics; Monte Carlo simulation; phase separation; wet spinning

INTRODUCTION

Developed by Leob and Sourirajan in late 1960s,[1] the nonsolvent-induced phase inversion process has now wide applications in both asymmetric membrane formation and fiber fabrication. In general four distinguishing structural elements have been reported, i.e., nodules, cellular structure, bicontinuous structure, and macrovoids. Among them macrovoids are undesirable because they are the roots of weak mechanical points and possibly lead to membrane failure under high pressures or continuously vibration.

Therefore, a large body of research has been done to understand the origins of morphological patterns, so as to minimize or eliminate macrovoids.[2–8] A milestone research of deriving analytical diffusion equations was initiated by Cohen and other scientists.[9–11] They first calculated the diffusion path in the ternary phase diagram, and pointed that composition dependence of the chemical potentials in the stable and metastable region was the formation criteria for two-phase structures structure. Smolders and Reuvers[12] categorized phase separation into delayed demixing and instantaneous demixing, and illustrated with calculated diffusion paths that macrovoids were associated with instantaneous demixing, except when the polymer additive concentration and the nonsolvent concentration in the polymer solution exceeded a certain minimum value. This was an elegant mechanism and widely accepted by membrane scientists. However the composition paths were theoretically calculated, while experimental concentration data were difficult to obtain because the phase separation process was completed in seconds or even shorter time.

Simulation methods have advantage in investigating the fast process of phase separation. Among them a notable computer simulation approach based on molecular motion was proposed by Termonia to develop a Monte Carlo diffusion model to study the diffusion processes and demixing processes in cast solution film.[13–15] Solvent/nonsolvent interaction was the key factor during the diffusion, which was in good agreement with some experiment results. Yet we believe that their work could be constructively improved if it had correlated the morphological development over time with composition paths in the thermodynamic equilibrium phase diagram. Another possible limitation of his work was that a polymer chain was coarse-grained as a single moving particle, and particles coagulated together as a movable cluster of entire rows, which neglected micro-Brownian motion of polymer segments. A simulation model that features microscopic movement of polymer segments would undoubtedly

Correspondence to: H. Zhang (zhanghd@fudan.edu.cn).
Contract grant sponsor: Major State Basic Research Development Program of China; contract grant number: 2011CB605700.
Contract grant sponsor: National High Technology Research and Development Program of China; contract grant number: 2008AA032101.
Contract grant sponsor: National Natural Science Foundation of China; contract grant number: 20990231.

reinforce its reliability. Zhou et al.[16] proposed a phase field model to simulate multiple kinetics phenomena such as diffusion and phase separation by using one set of ternary Cahn–Hilliard equations. Kyu et al.[17] adopted a time-dependent Ginzburg-Landau equation (TDGL) and discovered that diverse morphologies was a direct consequence of the initial conditions of the starting mixtures in a manner governed by the relative rates of solvent/nonsolvent exchange and the dynamics of phase separation. However some distinguishing structures such as finger-like macrovoid could not be revealed by their work due to the limitation of phase field model.

In this manuscript we adopt a novel Monte Carlo simulation model to study the coagulation process in wet spinning process, because relatively less studies are devoted to the fiber fabrication compared to those to polymeric membranes formation. Features of our model are elaborate motion of polymer segments and considering of kinetic parameters. A molecular model of 20 self-avoid walking segments is adopted in simulation.

Our simulation results have revealed that polymer/solvent/nonsolvent kinetic parameters, together with thermodynamic parameters, determine ultimate fiber morphology. On the basis of our systematical simulation, we propose a possible mechanism to explain the formation of ultimate fiber structures in wet spinning process, and we believe it can be applied to membrane formation system as well.

SIMULATION MODEL

Our approach is limited to a two-dimensional geometry similar to that encountered in typical wet spinning process. Two-dimensional model can be treated as a random cross section from real three dimension process as adopted in earlier work,[13–16] while simulation with 3D model is still under our research as this model requires a huge computer cost. During wet spinning process, cast solution is squeezed from a spinneret into coagulant bath. In our model, a square of 1000 × 1000 sites represents cross section of coagulation bath, and in its center the circular area with radius of 300 sites represents fiber cross section. Size of a single site is estimated to be size of polymer segment of 20 nm in diameter, which leads to fiber with initial diameter of 1.2×10^{-5} m, and ultimate diameter in the range of 10^{-6}–10^{-5} m, in accordance with experimental parameters. Local environment of micro-diagram is schematically demonstrated in Figure 1, where the curve shown should be treated as part of a circle. In the circle, the polymer solution is represented by a lattice of sites which are filled in by either solvent or a polymer segment, according to the polymer weight fraction.

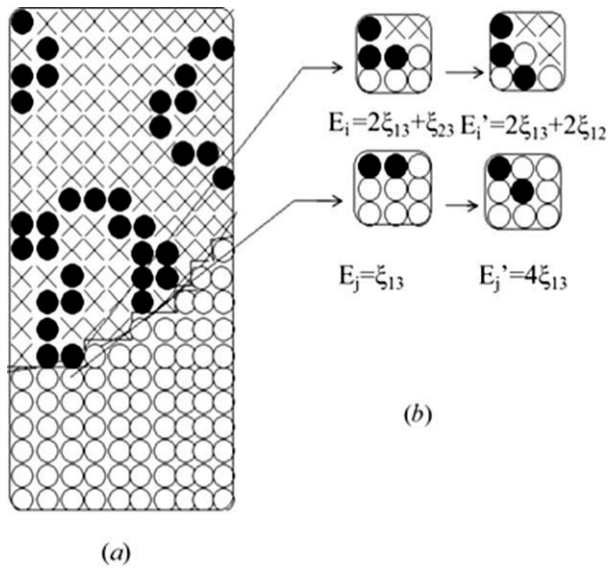

Figure 1 (a) schematic illustration of our simulation model for diffusion of a coagulant into a polymer solution. The polymer, the solvent and the coagulant particles are denoted by symbols ●, ×, ○ respectively. (b) The interaction energies of a particle with nearest neighbor particles before and after the exchange, where ζ_{13}, ζ_{12}, ζ_{23} denote interaction energies of nonsolvent/polymer, nonsolvent/solvent, solvent/polymer pairs.

The sites outside the circle are filled in with coagulant particles. A polymer chain is represented by a model consisting of 20 self-avoid walking segments, which fully reflects the random self-avoiding walk of polymer segments with a justifiable computer cost. We assume that the coagulating bath is infinite; therefore, solvent particles diffusing into the bath are removed from the lattice and replaced by coagulant particles. Coagulant, solvent and polymer particles are referred to by indexes 1, 2, and 3, respectively.

Following is the simulation process for phase separation. First we pick a random pair of particles i and j on nearest neighbor lattice sites. Within the local environment α for that pair, the rate for an exchange ij to ji is calculated from[18,19]

$$v_{ij\rightarrow ji,\alpha} = \tau_{i,j}^{-1} \exp(\beta \Delta E_\alpha/2) \tag{1}$$

in which energy change through the move is

$$\Delta E_\alpha = (E_i' + E_j') - (E_i + E_j) \tag{2}$$

and unit exchange time $\tau_{i,j}$ is related to the mutual diffusion coefficient $D_{i,j}^{\infty}$ at infinite dilution through

$$D_{i,j}^{\infty} = \tau_{i,j}^{-1} (\delta x)^2 \tag{3}$$

where δx is the unit lattice length. Then a probability for exchange is obtained through

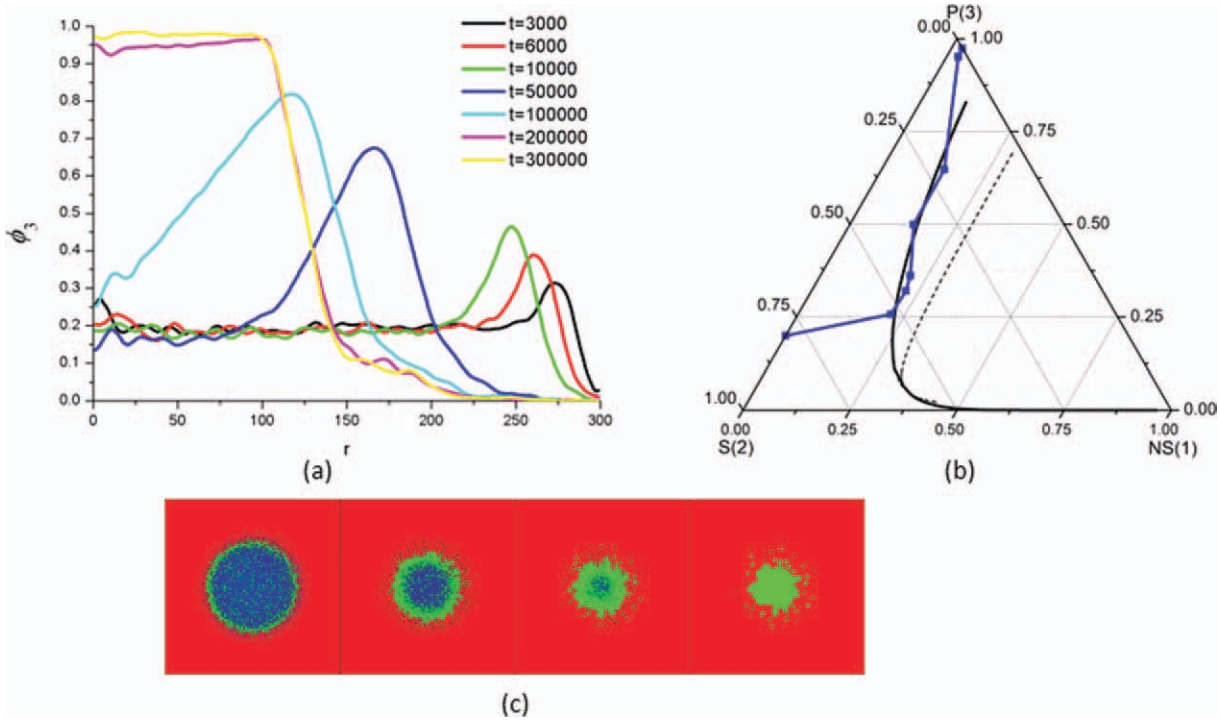

Figure 2 Case 1: (a) Composition profile evolution along the filament radius. (b) Composition path in phase diagram. (c) Cross sections of wet spinning fiber at 3000, 100,000, 200,000, 300,000 Monte Carlo Cycles. [Color figure can be viewed in the online issue, which is available at wileyonlinelibrary.com.]

$$P_{ij\to ji,\alpha} = v_{ij\to ji,\alpha}/v_{\max} \tag{4}$$

in which $v_{\max}$ denotes the highest rate of exchange among all the pairs on the lattice. A random number is generated, and if it falls below the probability for an exchange *ij* to *ji* the move *ij* to *ji* is allowed. After pick of each pair in the lattice the overall simulated time is incremented by t_{max}, which denotes the maximum time required for a pair change.

In addition to the single-site bond fluctuation algorithm,[20,21] we adopt modified slithering snake algorithm by Qing[22] as well. In this algorithm several segments of the polymer can move cooperatively as the effect of tensile force in the polymer chain. Because the tensile force can only transmit to slack segment, the slithering snake motion transmits along polymer chains till the nearest slack segment, rather till the end of chain as was thought before, so as to avoid artificial polymer chain over-shrink.

RESULTS AND DISCUSSION

Process controlled by thermodynamics parameters

Now we study the effect of interaction energies on phase separation in wet spinning process. It is crucial to determine proper thermodynamic parameters per simulation model. Our model consists of nonsolvent, solvent particles and polymer chains of 20 segments; according to Flory-Huggins theory[23] we have critical interaction parameter of two components:

$$\chi_c = \frac{1}{2}\left(\frac{1}{N_A^{1/2}} + \frac{1}{N_B^{1/2}}\right)^2 \tag{5}$$

where χ_c denotes critical interaction parameter, and N_A,N_B denote number of segments in each of the two interacting molecules. Resultantly critical interaction parameters of solvent-polymer and nonsolvent–polymer are 0.7, and that of solvent–nonsolvent is 2 in square lattices. Therefore, Flory-Huggins parameters χ_{12}, χ_{23}, and χ_{13}, i.e., pair interaction of solvent–nonsolvent, solvent–polymer, and nonsolvent–polymer, should be chosen below 2, below 0.7, and above 0.7, respectively. In our model, $\chi_{23} = 0.0$ ensures good miscibility between polymer and solvent, and $\chi_{13} = 1.8$ warrants immiscibility between polymer and nonsolvent. Enlightened by earlier work that morphologies are controlled by the pair interaction between solvent and coagulant,[13] in this part we choose a series of values for it in systematical simulation experiments. The results illustrate that three sets of thermodynamic parameters produce typical fiber morphologies and here we name them Case 1, Case 2, and Case 3. After we estimate the pair interaction parameters, equilibrium phase diagrams can be calculated according to the methods introduced by Ref. 24.

In terms of estimation of the kinetic parameters t, Termonia et al. 14 have done estimation below. Because the mutual diffusion coefficient of liquids is

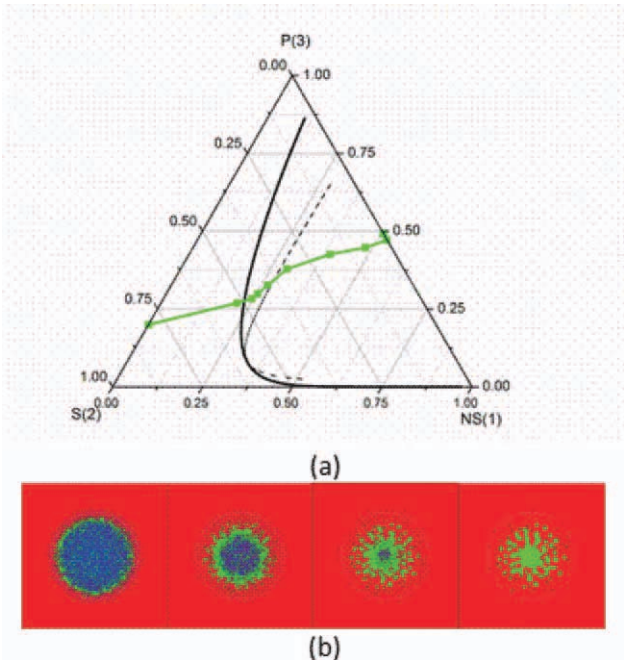

Figure 3 Case 2: (a) composition path in phase diagram. (b) Cross sections of wet spinning fiber at 3000, 100,000, 200,000, 300,000 Monte Carlo Cycles. [Color figure can be viewed in the online issue, which is available at wileyonlinelibrary.com.]

of the order of 10^{-5} cm^2 s^{-1}, use of eq. (3) leads to $\tau_{12} = 4.0 \times 10^{-7}$ s. The zero-concentration diffusion coefficient of most polymers in good solvents lies in the range 10^{-7}–10^{-6} cm^2 s^{-1}. Taking $D = 10^{-6.5}$cm^2 s^{-1} leads to $\tau_{13} = \tau_{23} = 1.3 \times 10^{-5}$ s. We follow their assumptions, and our model predicts fiber morphological development within seconds after immersion.

Figures 2–4 display fiber morphological development over time. Case 1 ($\chi_{23} = 0.0$, $\chi_{12} = 1.5$, $\chi_{13} = 1.8$) describes delayed demixing in which a dense sponge-like morphology is formed. Figure 2(a) presents concentration profiles along the radius from the center of fiber. From the coagulant/polymer interface toward the uncoagulated polymer solution, the following observations can be made: polymer concentration at the interface increases over time, and the concentration peak moves towards the center of filament, which indicates that the fiber surface shrinks as the nonsolvent immerses towards the cast solution and polymer chains continuously coagulate. Equilibrium phase diagram in Figure 2(b) shows that compositional path hardly touches bimodal curve, and almost stays in the single phase region. In an infinitely long delay time, polymers congregate into film at the boundary, which results in a dense filament. Figure 2(c) consists of four cross sections of wet spinning fiber at different computational time. As introduced in Simulation Model, each cross section is of the size 1000 × 1000 sites, and the fiber is of the diameter $10\times^{-5}$ m. Red, blue, green sites represent in sequence nonsolvent, solvent, and polymer. We can perceive that polymer in casting solution congregates toward the center of filament during the phase separation process.

In Case 2 ($\chi_{23} = 0.0$, $\chi_{12} = 1.0$, $\chi_{13} = 1.8$), as soon as the polymer solution is immersed into the coagulation bath, the fast solvent–coagulant exchange across the interface combined with the large repulsive forces between polymer and nonsolvent particles causes an immediate precipitation. However, complete precipitation is difficult to obtain practically in mixture of solution and coagulant, and polymer poor domains gradually grow into a finger-like structure.

Case 3 ($\chi_{23} = 0.0$, $\chi_{12} = 0.0$, $\chi_{13} = 1.8$) describes an instantaneous demixing process, and composition path traverses both binodal and spinodal curves at an early stage of phase separation after immersion (Fig. 4). Solvent particles in solution tend to be replaced by nonsolvent particles by virtue of good miscibility, and phase separation in such cases produces dust-like structures.

In the next section we would discuss how the kinetic parameters affect the fiber morphologies in each aforementioned case.

Process controlled by kinetic parameters

Effects of solvent–nonsolvent exchange rate

The rate of nonsolvent diffusion is controlled by t_{12}, i.e., the time required for solvent–nonsolvent

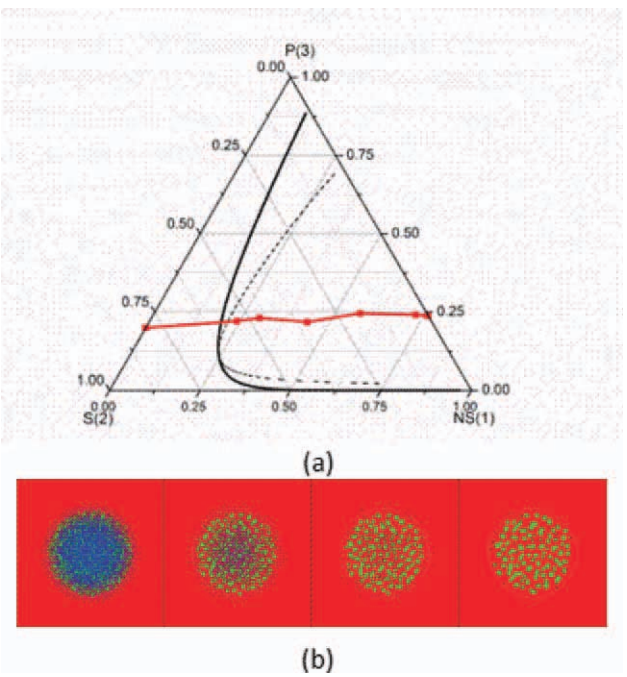

Figure 4 Case 3: (a) Composition path in phase diagram. (b) Cross sections of wet spinning fiber at 3000, 100,000, 200,000, 300,000 Monte Carlo Cycles. [Color figure can be viewed in the online issue, which is available at wileyonlinelibrary.com.]

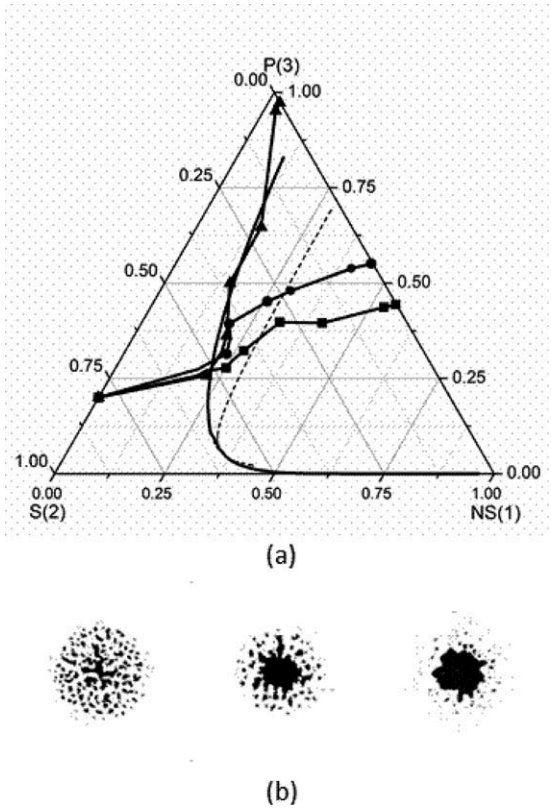

Figure 5 (a) Composition paths in phase diagram: ■, ●, ▲ represent τ_{12} in Case 1 changed from 1×10^{-7}, to 2×10^{-7}, and to 4×10^{-7} s. (b) Cross sections of wet spinning fiber at 300,000 Monte Carlo Cycles.

exchange. Figures 5–7 show the simulated solution/coagulant interface for a 20% polymer within seconds after precipitation in solvent. Black sites in cross sections represent ultimate polymer fibers; white area is occupied by nonsolvent which is washed away in practical experiment; solvent is not shown since it is expelled during demixing process. In ternary phase diagrams compositional paths with higher τ_{12} tend to cross the binodal curves at a later stage during phase separation, producing a denser fiber structure; while paths with smaller τ_{12} move toward phase separation regions and enter the regions in less than 0.1 s, resulting in a more porous structure. Such results are supported by Smolders' conclusion from calculation and experiment results that usually membranes without macrovoids are formed in case of delayed demixing, and membranes with macrovoid are formed in case of instantaneous demixing.[12] Our work reveals the interface composition change over time from statistical simulation results for the first time.

Although in most cases, void-free morphology can be obtained by selecting of proper τ_{12}, an exception is shown in Figure 7. It should be explained by competition of τ_{12} and τ_{13}: though in usual cases the diffusion of polymer into coagulant bath is ignorable compared to that of solvent particles into bath because of much lower mobility of polymer segments, in Case 3 its diffusion into the coagulant bath cannot be ignored, because an unusually slow solvent–nonsolvent exchange ($\tau_{12} = 0 \times 10^{-6}$ s and 4.0×10^{-6} s) is only one magnitude faster than polymer–nonsolvent exchange ($\tau_{13} = 1.0 \times 10^{-5}$ s).

Inspection of our simulation results leads to the following insight into the origin of the different structures. Upon immersion of the polymer solution in the coagulation bath, the nonsolvent penetrates into cast solution, rendering the system to an unstable situation, and resulting in congregation of the polymer at the interface. If the penetrating is too fast (denoted by very small value of τ_{12}), regions of uncoagulated polymer solution are bypassed by the penetration fronts. Those separated regions coagulate relatively more slowly and, hence, eventually form dust-like structure. If the immersion is, on the contrary, slow enough (τ_{12} value big enough) to allow complete segregation of polymer segments, a very dense polymer structure is obtained in which the coagulant forms spherical pores (sponge-like structure) behind the skin.

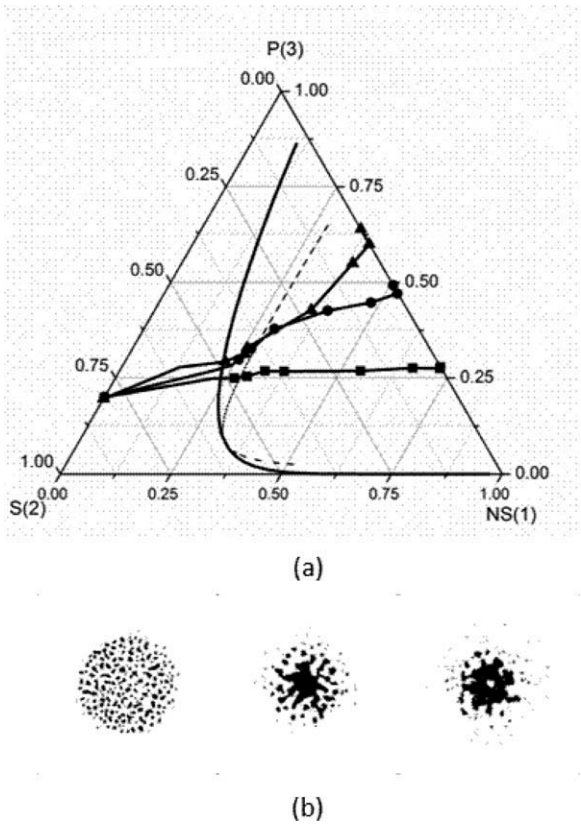

Figure 6 (a) composition paths in phase diagram: ■, ●, ▲ represent τ_{12} in Case 2 changed from 1×10^{-7}, to 4×10^{-7}, and to 1×10^{-6} s. (b) cross sections of wet spinning fiber at 300,000 Monte Carlo Cycles.

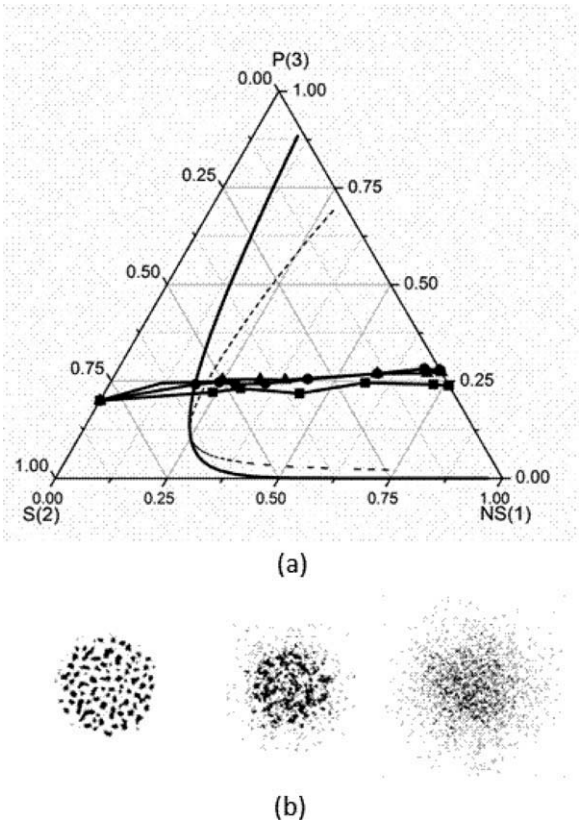

Figure 7 (a) Composition paths in phase diagram: ■, ●, ▲ represent τ_{12} in Case 3 changed from 4×10^{-7}, to 2×10^{-6}, and to 4×10^{-6} s. (b) Cross sections of wet spinning fiber at 300,000 Monte Carlo Cycles.

Effects of polymer–solvent exchange rate

We now turn to study the effect of polymer mobility, which is controlled by τ_{23}, the exchange rate between polymer and solvent. Figures 8–10 illustrate fiber morphologies get representative patterns from dusk-like to finger-like, and then to sponge-like in the three cases respectively with increasing polymer mobility. It is shown in equilibrium diagrams when τ_{23} is small, concentration paths enter phase separation regions at a late stage. The delay time is also observed in the turbidity measurements by Smolders,[12] during which polymers congregate toward the film and solvent is expelled from the film. Given a higher $\tau_{23,}$ the concentration path of the polymer moves toward the metastable region and enters it in a very short time (less than 0.1 s), corresponding to instantaneous turbidity in Smolders' experiment.

Results above reveal from a different aspect the origin of the different fiber structures. At a given coagulant penetration rate, if the mobility of polymer is high enough to coagulate into the polymer rich phase, a dense structure tends to form; on the contrary a low polymer mobility renders a relatively porous structure; correspondingly a finger-like structure develops if the polymer mobility is in-between.

On the basis of our systematical experiments above here we propose the mechanism that a competition of both factors of polymer mobility and coagulant immersion determines the ultimate fiber structure; not one of them plays a decisive role as was thought before. This mechanism offers explanations to phenomena including both our simulations and other well-known discoveries. For example, Smolders[12] found that in CA–acetone–water system, dioxane of a volume fraction over 0.15 in coagulant restrained macrovoids, and Strathmann[6] also observed that some solvent in coagulant helped to control the formation of macrovoids. It would be interpreted that a decrease of nonsolvent volume fraction in coagulant results in a decreased chemical potential gap between the solution and coagulant, i.e., the motivation and kinetics for phase separation, in

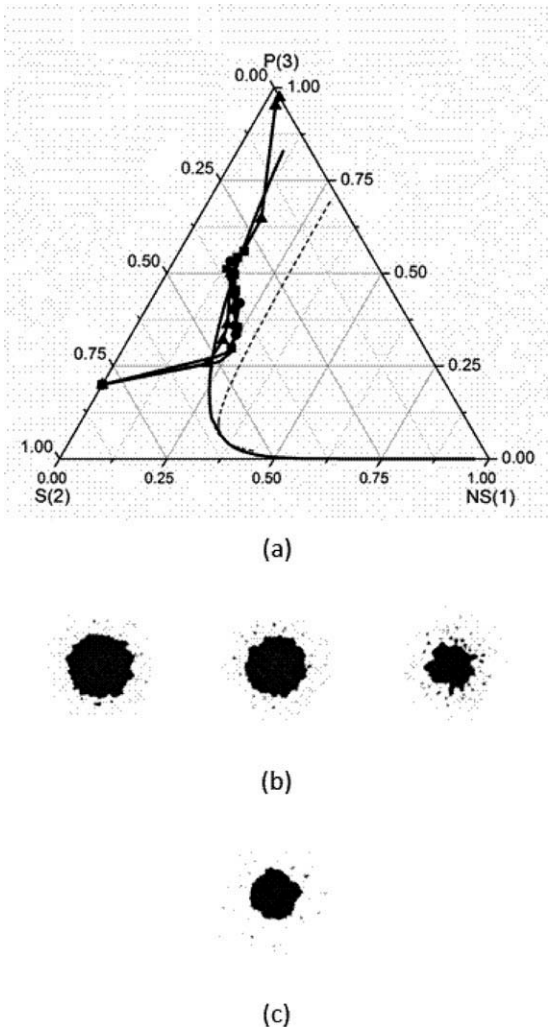

Figure 8 (a) Composition paths in phase diagram: ■, ●, ▲ represent τ_{23} in Case 1 changed from 8×10^{-4}, to 2×10^{-4}, and to 1.3×10^{-5} s. (b) Cross sections of wet spinning fiber at 300,000 Monte Carlo Cycles. (c) cross sections of wet spinning fiber with τ_{23} of 8×10^{-4} s and same thermodynamics as Case 1 at 1,500,000 Monte Carlo Cycles.

which case polymer chains have enough time to coagulate and a dense structure would form according to our mechanism.

It is interesting to notice in the left two graphs of Figure 8(b) a skin-core structure forms when τ_{23} is extremely high (about three magnitudes higher than τ_{12}). It should be interpreted by that very poor mobility of polymer causes slowdown of the phase separation process, and the interpretation is reinforced by a dense structure obtained at a longer time [see Fig. 8(c)].

Effect of polymer–nonsolvent exchange rate

Finally we turn to study the effect of polymer/solvent exchange on ultimate fiber structures. Results with varied τ_{13} are presented in Figure 11 for an estimated coagulation time around 0.03 s. It is conspicuous that with a small value of τ_{13}, three systems present a similar trend of polymer molecules diffusing into coagulant bath. Such a trend is easily understood: shortening of t_{13} decreases the difference between τ_{13} and τ_{12}. To be specific, when τ_{13} (1.3×10^{-5} s) is two magnitude higher than τ_{12} (4.0×10^{-7} s), polymer chains move much slower than solvent, so the polymer diffusion into bath is ignorable; however when τ_{13} (3.0×10^{-6} s) is about the same magnitude with τ_{12} (4.0×10^{-7} s), the chance of polymer exchanging with nonsolvent becomes higher. If we increase τ_{13}, the filaments in three systems are more porous. Also interpreted from a view of competing τ_{13} and τ_{12}, inhibition in polymer exchange with nonsolvent increases the chance that solvent exchanges with nonsolvent, resulting in porosity in fiber structures. This competition is another determinant factor in fiber morphology formation and of less importance because in practical experimental system there exists a tendency for phase separation between polymer and non-solvent and consequently their chance of exchange is quite low.

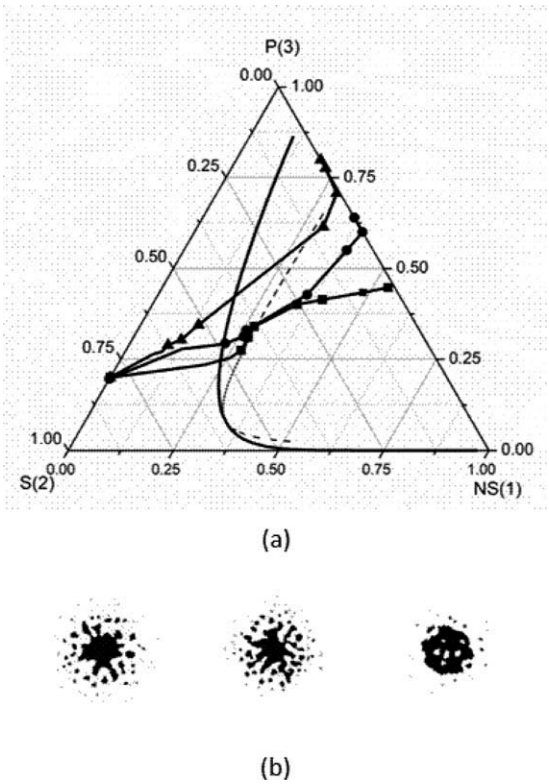

Figure 9 (a) composition paths in phase diagram: ■, ●, ▲ represent τ_{23} in Case 2 changed from 5×10^{-5}, to 1.3×10^{-5}, and to 3×10^{-7} s. (b) Cross sections of wet spinning fiber at 300,000 Monte Carlo Cycles.

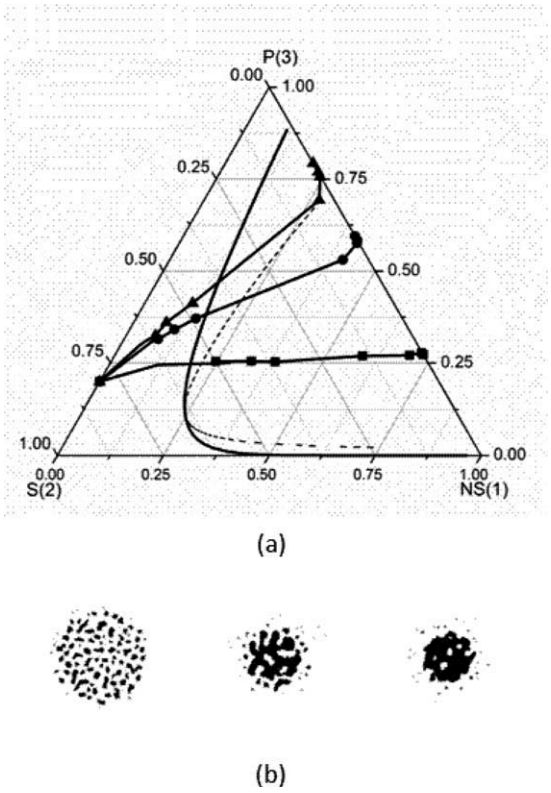

Figure 10 (a) composition paths in phase diagram: ■, ●, ▲ represent τ_{23} in Case 3 changed from 1.3×10^{-5}, to 1×10^{-6}, and to 3×10^{-7} s. (b) Cross sections of wet spinning fiber at 300,000 Monte Carlo Cycles.

CONCLUSIONS

We have improved a Monte Carlo model for the study of the morphological development during wet spinning process. Introducing a molecular model consisting of 20 polymer segments which fully reflects the polymer motion permits the study of effects of kinetic parameters on fiber structures. By varying binary exchange rate between particles, we reproduce various polymer structures ranging from dust-like, finger-like to sponge-like morphologies. On the basis of our systematical experiments we propose the mechanism that a competition of both

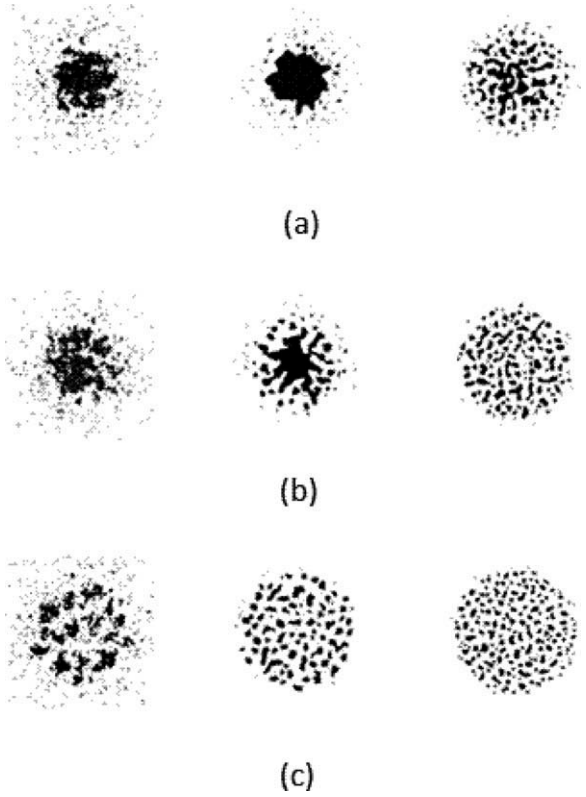

Figure 11 Cross sections of wet spinning fiber with $\tau_{13} = 3 \times 10^{-6}$, 1.3×10^{-5}, 5×10^{-5} s in sequence at 300,000 Monte Carlo Cycles : (a) Case 1, (b) Case 2, (c) Case 3.

factors of polymer mobility and coagulant immersion is the determinant factor of ultimate fiber structure. It is applicable to membrane formation as well.

References

1. Loeb, S.; Sourirajan, S. Adv Chem Ser 1963, 38, 117.
2. Matz, R. Desalination 1972, 10, 1.
3. Frommer, M. A.; Messalam, R. M. Ind Eng Chem Prod Res Dev 1973, 12, 328.
4. Sterling, C. V.; Scriven, L. E. AIChE J 1959, 5, 514.
5. Ray, R. J.; Kranz, W. B.; Sani, R. L. J Membr Sci 1985, 23, 155.
6. Strathmann, H.; Kock, K.; Amar, P.; Baker, R. W. Desalination 1975, 16, 179.
7. Craig, J. P.; Knudsen, J. P.; Holland, V. F. Text Res J 1962, 32, 435.
8. Broens, L.; Altena, F. W.; Smolders, C. A. Desalination 1980, 32, 33.
9. Cohen, C.; Tanny, G. B.; Prager, S. J Polym Sci Part B: Polym Phys 1979, 17, 477.
10. Reuvers, A. J.; Vandenberg, J. W. A.; Smolders, C. A. J Membr Sci 1987, 34, 45.
11. Tsay, C. S.; McHugh, A. J. J Polym Sci Part B: Polym Phys 1990, 28, 1327.
12. Smolders, C. A.; Reuvers, A. J.; Boom, R. M.; Wienk, I. M. J Membr Sci 1992, 73, 259.
13. Termonia, Y. Phys Rev Lett 1994, 72, 3678.
14. Termonia, Y. J Polym Sci Part B: Polym Phys 1995, 33, 279.
15. Termonia, Y. J Polym Sci Part B: Polym Phys 1998, 36, 2493.
16. Zhou, B.; Powell, A. J Membr Sci 2006, 268, 150.
17. Dayal, P.; Kyu, T. Macromol Symp 2007, 258, 170.
18. Alexandrowicz, Z. J Chem Phys 1969, 51, 561.
19. Metropolis, N.; Rosenbluth, A. W.; Rosenbluth, M. N.; Teller, A. H.; Teller, E. J Chem Phys 1953, 21, 1087.
20. Larson, R. G.; Sciven, L. E.; Davis.H. T. J Chem Phys 1985, 83, 2411.
21. Lu, J. M.; Yang, Y. L. Sci China Ser A 1991, 34, 1226.
22. Qin, Y.; Liu, H. L.; Hu, Y. Chem J Chin Univ 2002, 23, 1447.
23. Flory, P. J. Principles of Polymer Chemistry; Cornell University Press: New York, 1953; Chapter 13, p 541.
24. Altena, F. W.; Smolders, C. A. Macromolecules 1982, 15, 1491.